Angewandte Chemie
Eine Zeitschrift der Gesellschaft Deutscher Chemiker

Supporting Information

Assembly of The Mitochondrial Complex I Assembly Complex Suggests a Regulatory Role for Deflavination

Gabriele Giachin[+], Matthew Jessop[+], Romain Bouverot, Samira Acajjaoui, Melissa Saïdi, Anaïs Chretien, Maria Bacia-Verloop, Luca Signor, Philippe J. Mas, Adrien Favier, Eve Borel Meneroud, Michael Hons, Darren J. Hart, Eaazhisai Kandiah, Elisabetta Boeri Erba, Alain Buisson, Gordon Leonard, Irina Gutsche, and Montserrat Soler-Lopez**

anie_202011548_sm_miscellaneous_information.pdf

Methods

DNA plasmids

The human DNA sequences coding for mitochondrial ECSIT ($ECSIT_{Mt}$, residues 49-431), ECSIT N-terminus ($ECSIT_{NTD}$, residues 49-252), ECSIT C-terminus ($ECSIT_{CTD}$, residues 247-431), mature ACAD9 (residues 38-621) and chimeric ACAD9 ($ACAD9_{VLCAD}$, replacement of ACAD9 residues 445-482 by VLCAD residues 481-518) were *E. coli* codon-optimized and synthesized by ShineGene Molecular Biotech. Mature NDUFAF1 (residues 25-327) and mature VLCAD (residues 75-655) were PCR-amplified from human cDNA clones (GE Healthcare plasmid #3504355 and Addgene plasmid #38838, respectively). All the other DNA sequences were inserted into the pET-21d(+) expression vector. To generate the Venus fragment-fused plasmids for BiFC assays, the DNA sequences of mitochondrial ECSIT, ECSIT N-terminus, ECSIT C-terminus and mature ACAD9 were inserted into the pBiFC-VC155 (Venus residues 155-238, A206K) or pBiFC-VN173 (Venus residues 1-172) vectors (Addgene plasmids #22011 and #22010, respectively). To generate the bait and prey plasmids for yeast two-hybrid assays, the coding DNA sequences for mitochondrial ECSIT, ECSIT N-terminus, ECSIT C-terminus, mature NDUFAF1, mature ACAD9 and full-length TRAF6 (residues 1-522) were inserted into both pEXP22 (prey) and pEXP32 (bait) vectors (ThermoFisher Scientific). All the constructs were obtained using restriction free cloning protocol[1].

Expression of soluble proteins by random incremental truncation (ESPRIT) library screening

DNA fragments encoding ECSIT residues 1-248, 1-269, 1-392, 1-404 and 1-431 were subcloned into pESPRIT002, downstream of an N-terminal TEV protease-cleavable His_6-tag and upstream and in-frame with a C-terminal biotin acceptor peptide (BAP) used as a marker of protein solubility and stability. Full methods and materials for ESPRIT have been detailed elsewhere[2]. A total of 14025 colonies (9405 for the N-terminal sub-library and 4620 for the C-terminal sub-library) were screened. Results are summarised in **Figure S2**.

Recombinant protein expression and purification

Mitochondrial ECSIT (residues 49-431), $ECSIT_{CTD}$ and NDUFAF1 were expressed in *E. coli* BL21 Star (DE3) cells (ThermoFisher Scientific) in 6 LB medium at 25 °C (for ECSIT proteins) and 16 °C (for NDUFAF1) and induced with isopropyl-β-D-galactopyranoside (IPTG) to a final concentration of 250 and 80 μM (for ECSIT proteins and NDUFAF1, respectively). ACAD9, VLCAD and chimeric $ACAD9_{VLCAD}$ were expressed in *E. coli* C43(DE3) cells (Lucigen) in 6 L Terrific Broth medium with 8 g/L glycerol at 37 °C and induced with 500 μM IPTG and harvested 12 hours after induction. Bacterial pellets were resuspended in lysis buffer (200 mM potassium phosphate buffer or PBS, 1 mM DTT, 0.25 mM EDTA, 0.2% Tween-20, pH 7.8) supplemented with protease inhibitor cocktails (Merck) and *DNase I* (Merck). Bacterial lysis was performed by sonication (QSonica), lysates were centrifuged for 30 min at 35,000 g (Avanti J-20 XP centrifuge, Beckman Coulter) and the supernatants were filtered (0.22 μm pore size filter) before protein purification.

The single proteins were purified by a combination of affinity and size-exclusion chromatography (SEC) performed on Äkta Purification systems (GE Healthcare). Typically, 0.5 L of the single protein soluble fractions was loaded onto a 5-mL HisTrap column (GE Healthcare) equilibrated in 200 mM PBS, 1 mM DTT, 0.5 mM EDTA, pH 7.8 and eluted with a linear imidazole gradient up to 500 mM imidazole in 200 mM PBS,

1 mM DTT, 0.5 mM EDTA, pH 7.8. Subsequently, the proteins were further purified by a combination of SEC columns. In particular, $ECSIT_{CTD}$ and NDUFAF1 were purified on a HiLoad Superdex 75 pg 16/600 and on a Superdex 75 10/300 GL SEC columns (GE Healthcare) with 25 mM HEPES, 250 mM NaCl, pH 7.5 as running buffer. Mitochondrial ECSIT, ACAD9 and VLCAD were purified on a HiLoad Superdex 200 pg 16/600 and on a Superdex 200 10/300 GL SEC columns (GE Healthcare) equilibrated with 25 mM HEPES, 250 mM NaCl, pH 7.5. Single protein identity was confirmed by electron spray ionization time-of-flight mass spectroscopy (ESI-TOF/MS). The MCIA complex formed by ACAD9 and $ECSIT_{CTD}$ was obtained by co-purification. The single proteins were expressed as previously described and the bacterial pellets were co-lysed and centrifuged together. The soluble fraction was loaded overnight onto a 5-mL His-Trap column equilibrated in 200 mM PBS, 1 mM TCEP, 0.5 mM EDTA, pH 7.8 and eluted with a linear imidazole gradient up to 500 mM imidazole in 200 mM PBS, 1 mM TCEP, 0.5 mM EDTA, pH 7.8. Subsequently, the proteins were concentrated using 100 kDa cut-off Amicon Ultra filters and purified by Sephacryl S300 HR 16/600 and Superose 6 10/300 GL SEC columns (GE Healthcare) equilibrated with 25 mM HEPES, 250 mM NaCl, 1 mM TCEP, pH 7.5. An identical protocol was followed to attempt the co-purification of VLCAD-$ECSIT_{CTD}$ and $ACAD9_{VLCAD}$-$ECSIT_{CTD}$ respectively. Single proteins and protein complexes were stored at 4 °C until use.

Size Exclusion Chromatography coupled to Multi-Angle Laser Light Scattering (SEC-MALLS)

The molecular mass of $ECSIT_{CTD}$, NDUFAF1 and ACAD9 in solution was determinate by SEC coupled to multi-angle laser light scattering (SEC-MALLS) using a Superdex 200 10/300 GL column equilibrated in buffer 25 mM HEPES, 250 mM NaCl, pH 7.8. The measurements were performed at 20 °C using 50 µL of proteins at 5 mg/mL with a flow rate of 0.5 mL/min and eluted proteins were monitored using a DAWN-EOS detector with a laser emitting at 690 nm for online MALLS measurement (Wyatt Technology Corp.) and with a RI2000 detector for online refractive index measurements (SchambeckSFD). Molecular mass calculations were performed with the ASTRA software using a refractive index increment (dn/dc) of 0.185 mL/g. Data were visualized using OriginPro 9.0 (OriginLab) software.

Differential Scanning Calorimetry (DSC)

The melting temperatures of $ECSIT_{CTD}$, ACAD9, VLCAD and the ACAD9-$ECSIT_{CTD}$ complex were determined by differential scanning calorimetry (DSC). Thermal denaturation experiments were carried out on a micro-DSC III microcalorimeter (Setaram Instrumentation). Protein solutions at 100 µM concentration were degassed under vacuum at 20 °C for calorimetric measurements. The DSC scans were run between 20 and 95 °C at a rate of 60 °C/hour. Reversibility of the unfolding transition was estimated by rescanning the sample from 95 to 20°C at the same rate. The denaturation temperature, T_m, corresponding to the maximum of the transition peak, was determined from 3 replicate runs and varied not more than 0.25 °C. The data were processed and analysed using the Thermal Analysis Software CALISTO (Setaram Instrumentation) and OriginPro 9.0 software for visualisation.

^{15}N-Heteronuclear Single Quantum Coherence (HSQC) NMR Spectroscopy

NMR experiments were performed on 0.5 mM ^{15}N-labelled $ECSIT_{CTD}$ and on 0.5 mM ACAD9-^{15}N-$ECSIT_{CTD}$ complex expressed and purified as described above. For isotope labeling 1 g/L [^{15}N] ammonium chloride was

added to 2 L of minimal medium. BEST TROSY experiments (^{1}H-^{15}N correlation spectra) and DOSY experiments (for measuring the translational diffusion) were recorded at 300 K on Bruker ADVANCE III HD spectrometers operating at ^{1}H frequency of 700 MHz and equipped with a triple resonance pulsed field gradient cryoprobe[3]. Data processing was conducted with either FELIX (Biosym Technologies) or NMRPipe[4].

Small Angle X-ray Scattering (SAXS) data collection and analysis

The experiments were performed at the ESRF BioSAXS beamline BM29, Grenoble, France[5]. $ECSIT_{CTD}$ and NDUFAF1 were measured in batch mode at 20 °C immediately after the protein purification. For these measurements, 45 µL of sample solution at three different concentrations (5, 2.5 and 1 mg/mL) were used. ACAD9-$ECSIT_{CTD}$ complex sample was measured in batch mode immediately after the SEC elution using 0.8, 1.2 and 2 mg/mL concentration dilutions. ACAD9 and VLCAD were measured by SEC-SAXS to separate larger protein aggregates. A volume of 250 µL of protein per each ACAD9 or VLCAD sample at 10 mg/mL was loaded on a Superose 6 10/300 GL column *via* a high performance liquid chromatography device (HPLC, Shimadzu, France) attached directly to the sample-inlet valve of the BM29 sample changer[6]. All the samples were measured in buffer 25 mM HEPES, 250 mM NaCl, pH 7.5 at 20 °C. The column was equilibrated with 3 column volumes to obtain a stable background signal that was confirmed before measurement. A flow rate of 0.5 mL/min was used for all sample measurements.

SAXS analysis of the overall parameters was carried out by PRIMUS from ATSAS 2.8.4 package[7] and by ScÅtter 3.0 software[8]. The pair distance distribution function, P(r), radius of gyration (R_g) and maximum diameter of the particle (*Dmax*) were calculated in GNOM using indirect Fourier transform method[9]. Protein molecular masses were estimated using both Porod volume[9] and scattering mass contrast[10] methods. For ACAD9, VLCAD and the ACAD9-$ECSIT_{CTD}$ complex the pair distance distribution functions were used to calculate *ab initio* models in C2 symmetry with DAMMIF, DAMMIN and GASBOR; the DAMMIF models were averaged, aligned and compared using DAMAVER[7]. The most representative *ab initio* DAMMIF models for ACAD9 and VLCAD were compared to the ACAD9 homology model and the VLCAD structure, respectively, aligned using SUPCOMB[11] and visualized using UCSF Chimera software[12]. All SAXS data were deposited into SASBDB data bank. All parameters for SAXS analysis, sample details and results are described in **Supplementary Table 1**.

Electrophoresis Mobility Assay - Native Polyacrylamide Gel Electrophoresis (native PAGE)

Purified proteins (ACAD9 and VLCAD at 16.8 µM) were incubated with increasing concentrations of $ECSIT_{CTD}$ (4.5 to 36 µM) for 30 min at room temperature in a buffer containing 25 mM HEPES pH 7.5, 50 mM NaCl, 1 mM TCEP. Similarly, $ECSIT_{CTD}$ at 12.5 µM was titrated with increasing NDUFAF1 concentrations (3.4 to 27 µM). Native electrophoresis was then carried out using a Mini-PROTEAN® TGX Stain-Free™ Precast Gels (5% acrylamide) (Bio-Rad) in 1x TBE buffer. Migration of proteins was visualized by Comassie Brilliant Blue (Sigma) staining.

Liquid Chromatography/Electrospray Ionization Mass Spectrometry (LC/ESI-MS)

LC/ESI-MS was performed on a 6210 TOF mass spectrometer coupled to a HPLC system (1100 series, Agilent Technologies). All solvents used were HPLC grade; the HPLC mobile phases were A (H_2O 95%, ACN 5%,

TFA 0.03%) and B (ACN 95%, H_2O 5%, TFA 0.03%). Protein samples were desalted on-line on a C8 reversed-phase micro-column (Zorbax 300SB-C8, 5 µm, 5 x 0.3 mm, Agilent Technologies) for 3 min at 50 µL/min with 100% of mobile phase A, then eluted at 50 µL/min with 70% of mobile phase B. MS acquisition was carried out in the positive ion mode in the 300–3000 *m/z* range and the data processed with MassHunter software (v. B.02.00, Agilent Technologies). The mass spectrometer was calibrated with tuning mix (ESI-L, Agilent Technologies). The mass spectrometer settings were the following: gas temperature (azote) 300 °C, drying gas (azote) 7 L/min, nebulizer gas (azote): 10 psig, Vcap: 4 kV, fragmentor: 250 V, skimmer: 60 V, Vpp (octopole RF): 250 V.

Native Mass Spectrometry (native MS)

The proteins were analysed by native MS in the concentration range of 3–5 µM. Macromolecular complexes formed by ACAD9 and $ECSIT_{CTD}$ were analysed by native MS[13, 14]. Protein buffer was freshly exchanged to 250 mM ammonium acetate. Protein ions were generated using a nanoflow electrospray (nano-ESI) source. Nanoflow platinum-coated borosilicate electrospray capillaries were bought from Thermo Electron SAS (Courtaboeuf, France). MS analyses were carried out on a quadrupole time-of-flight mass spectrometer (Q-TOF Ultima, Waters Corporation). The instrument was modified for the detection of high masses[15]. The following instrumental parameters were used: capillary voltage = 1.2–1.3 kV, cone potential = 40 V, RF lens-1 potential = 40 V, RF lens-2 potential = 1 V, aperture-1 potential = 0 V, collision energy = 30–140 V, and microchannel plate (MCP) = 1900 V. All mass spectra were calibrated externally using a solution of caesium iodide (6 mg/mL in 50% isopropanol) and were processed with the Masslynx 4.0 software (Waters Corporation, Manchester, U.K.) and with Massign software package[16].

Negative stain Electron Microscopy (ns-EM)

ACAD9 protein sample at 0.05 mg/mL was applied to a carbon/mica interface. The carbon layer was subsequently floated onto a 2% sodium silicotungstate solution (pH 7.4), recovered with a 400 mesh copper grid (Agar) and air dried for 1 minute. Micrographs were taken under low-dose conditions (exposing for 1 s at an electron dose of 20 $e^-/Å^2$) on a Tecnai 12 LaB6 microscope (FEI) operated at 120 kV. Images were recorded with a Gatan Orius 1000 CCD camera at a nominal magnification of 22000 x, corresponding to a pixel size of 3.24 Å/pixel on the specimen level, with a defocus between 1.2 and 2.5 µm. CTF estimation was carried out using CTFFIND4[17], and particles were selected using the LoG picking algorithm implemented in RELION-3[18]. 92,410 particles were extracted with a box size of 100 x 100 pixels and subjected to several rounds of 2D classification in RELION-3, resulting in a cleaned particle set of 79,924 particles. From these particles 39,795 particles from classes with isolated ACAD9 dimers (i.e. with no close neighbouring particles) were used to generate an initial model with applied C2 symmetry using the initial model generation algorithm in RELION-3. All 79,924 particles were then refined against this initial model with applied C2 symmetry, with a loose mask to remove the contribution from neighbouring ACAD9 dimers, resulting in the negative stain EM envelope shown in **Figure S5A-B**.

Cryo-Electron Microscopy (cryo-EM), data acquisition, processing and 3D reconstruction

Quantifoil R 2/1 Cu/Rh 300 mesh holey carbon grids were pumped under vacuum for 1 hour and glow discharged at 45 mA for 20 s. 4 µL of ACAD9-ECSIT$_{CTD}$ were deposited on the grid and vitrified with a Vitrobot Mark IV (FEI). 7,510 movies of 40 frames were collected using EPU (Thermo Fisher) on a Titan Krios microscope equipped with a K2 Summit camera (Gatan) at the CM01 ESRF facility[19]. Images were collected with a total electron dose of 41 $e^-/Å^2$, at a nominal magnification of 131,000 x which corresponds to a pixel size of 1.067 Å/pixel at the specimen level, with ~50% of images collected with a 30º tilt to counteract the strong preferential orientation observed while screening grids. Motion correction was carried out using MotionCor2[20] and the CTF was corrected using GCTF[21]. Micrographs with an estimated resolution in GCTF of better than 8 Å were retained and manually screened by eye, resulting in 2,999 micrographs used for further processing. 2,901 particles were manually picked from a subset of micrographs using the Boxer program in EMAN[22], extracted with a box size of 160 x 160 pixels and subjected to 2D classification in RELION-2.1[23]. The best 2D classes were then used as templates for auto-picking in RELION, on a larger subset of the data. This resulted in ~490,000 picked particles, which were then extracted and subjected to several rounds of 2D classification. The best 2D class averages were then used as templates for GPU-accelerated picking in Gautomatch (http://www.mrc-lmb.cam.ac.uk/kzhang/) on all micrographs. The coordinates of the resulting ~700,000 picked particles were used as input for per-particle CTF correction in GCTF. Particles were then imported into CryoSPARC[24] for further processing.

2D and 3D classification were extensively employed to find a stable subset of particles which yielded a map consistent with the secondary structural features seen in both 2D class averages and the VLCAD-based ACAD9 homology model. The contribution of ECSIT$_{CTD}$, coupled with the strong preferential orientation of the complex, complicated the image analysis process. Many different trials were carried out as described in the **Figure S7**.

We first focussed only on the ACAD9 core of the ACAD9-ECSIT$_{CTD}$ complex, in order to avoid misalignment due to the highly disordered ECSIT$_{CTD}$. Particles were subjected to several rounds of 2D classification with high initial uncertainty factors. ~16,000 particles from the 2D class averages showing the strongest secondary structural features of the ACAD9 core were selected and subjected to *ab initio* 3D reconstruction with applied C2 symmetry. The resulting volume was then used to create a mask using the Volume Tools utility in CryoSPARC. This mask was applied during homogeneous refinement with imposed C2 symmetry against the *ab initio* volume, resulting in a map with an estimated resolution of 7.8 Å after sharpening with a B-factor of -500 $Å^2$. Rigid body fitting of the VLCAD-based homology model of ACAD9 into the cryo-EM map of the ACAD9-ECSIT$_{CTD}$ complex core was then carried out in Chimera[12].

For the full map of ACAD9-ECSIT$_{CTD}$, particles were split into 6 equal subsets. Each subset was subjected to *ab initio* reconstruction into 5 classes with no applied symmetry. This consistently resulted in one class with dimensions agreeing with features of the 2D classes, and four junk classes. Particles from the best *ab initio* 3D class from each subset were combined, resulting in ~240,000 particles which were subjected to several rounds of 2D classification. ~36,000 particles from the 6 best 2D class averages which showed different

orientations were used for *ab initio* reconstruction with no applied symmetry into two classes. Particles from the best class were then subjected to non-uniform refinement with applied C2 symmetry, resulting in a map that possessed an ACAD9 core that was consistent with the homology model and displayed notable protrusions near the vestigial dehydrogenase of ACAD9, which are attributed to $ECSIT_{CTD}$. Particles were then refined against this map in RELION with applied C2 symmetry, resulting in a map filtered to 15 Å resolution to focus on the global envelope of the ACAD9-$ECSIT_{CTD}$ complex in order to visualize the $ECSIT_{CTD}$ binding site.

Limited proteolysis

Limited proteolysis of proteins was carried out by adding trypsin proteolytic enzyme (Sigma). ACAD9, VLCAD and $ACAD9_{VLCAD}$ at 1 mg/mL were incubated with trypsin at 1:10000 ratio in absence or presence of $ECSIT_{CTD}$ (at 5 mg/mL) at room temperature for 30 minutes. The incubated mixtures were then mixed with SDS gel loading dye, boiled prior to their resolution by a SDS-15% PAGE and stained with Coomassie brilliant blue (Sigma).

Yeast two-hybrid (Y2H) interaction assays

Bait and prey plasmids were pairwise co-transformed into MaV203 yeast strain (kindly provided by Dr. Ulrich Stelzl, University of Graz, Austria) as previously reported[25], plated onto selective SD2 (lacking Leu and Trp amino acids) agar media and incubated for 72 hours at 30°C to detect colony growth. Co-transformant arrays were then replica-cleaned before being plated onto different selective media for interaction screening. To assay the activation of the HIS3 reporter gene, SD3 (lacking Leu, Trp, His) agar plates were supplemented with 15 to 50 mM of 3-aminotriazole (3AT, Sigma). Colony growth was inspected after 6-7 days of incubation. A previously reported interaction between ECSIT and TRAF6 was used as a positive control[26].

Bimolecular Fluorescence Complementation (BiFC) assays

HEK293 cells were grown in Dulbecco's modified eagle medium containing 10% fetal bovine serum, 10,000 units/mL penicillin and 10,000 µg/mL streptomycin at 37 °C in a humidified atmosphere containing 5% CO_2. The day before transfection, HEK293 cells were plated on 12-well plates with OPTI-MEM medium (ThermoFisher Scientific). The cells were co-transfected with 0.2 µg of BiFC probes and the actin filament marker LifeAct-RFP using Lipofectamine transfection agent (ThermoFisher Scientific). LifeAct-RFP is a cell marker through the labelling of actin with Red Fluorescent Protein (RFP). The cellular intensities of BiFC fluorescence were analysed 48 hours after transfection using the FITC (green spectrum) and estimated as the ratio of FITC vs colocalised CY3.5 (red spectrum). Each experiment was performed as triplicate.

Detection of FAD content by UV-vis Spectroscopy

The estimation of FAD content in ACAD9 and in the ACAD9-$ECSIT_{CTD}$ complex was performed using UV-vis spectrophotometer (UV-2401PC, Shimadzu) at 16 µM protein concentration in buffer 25 mM HEPES, 250 mM NaCl, pH 7.5. Absorbance spectra were recorded with 1 nm steps within a wavelength range from 300 nm to 550 nm using a 10 mm light path quartz cuvette. To test FAD quenching, decanoyl-CoA (Sigma) was added to the samples at different molar ratio (i.e. 1:1, 3:1, 10:1 and 20:1) and spectra were recorded within a wavelength range from 300 nm to 550 nm as before. All the UV-vis measurements were carried at 20 °C and in triplicate. Data were processed and visualized using OriginPro 9.0.

Acyl-CoA dehydrogenase (ACAD) activity assay

We used the ETF fluorescence reduction assay for sensitive, accurate determination of ACAD activities, since ETF is the natural electron acceptor for the ACAD enzymes[27]. The plasmids of the human electron transfer flavoprotein ETF-alpha and ETF-beta subunits were a gift from Pal Falnes (pF710-pETDuet-1-Hs-delta19-ETFalpha-noHis and pF709-pET28a-Hs-FL-ETFbeta-NHis, Addgene plasmids #85110 and #85110 respectively). Purification of the recombinant ETF alpha/beta heterodimer was carried out as described in[28]. Briefly, *E. coli* C43(DE3) cells (Lucigen) were co-transformed with the plasmids, induced with 500 µM IPTG and harvested 12 hours after induction at 37ºC. Cells were lysed in lysis buffer (20 mM NaH_2PO_4, 0.05% Tween-20, pH 7.5) supplemented with lysozyme (Merck), protease inhibitor cocktails (Merck) and *DNase I* (Merck). Cleared lysates were loaded onto a 5-mL HisTrap column (GE Healthcare) equilibrated in 20 mM NaH_2PO_4, pH 7.5. Bound proteins were eluted with equilibration buffer supplemented with 500 mM imidazole. Elution fractions containing ETF heterodimer were pooled, dialysed against 50 mM Tris, pH 8.0, 5% glycerol and purified on a Superdex 200 10/300 GL SEC column (GE Healthcare). Purified samples were stored at -80 ºC.

Anaerobic ETF fluorescence reduction assays were done as described in[27], with reaction volumes of 200 µL in Elplasia black-walled 96-well plates (Corning). Reactions were measured in an Infinite M200 PRO reader (TECAN) set to 32 °C, using Ex340/Em490. 30 data points were collected for each sample over a 1min measurement window. Glucose oxidase (Sigma G2133, ~20U/mL final concentration) and catalase (Sigma C30, 0.5 µL/mL final) were added and fluorescence was zeroed (Ex340/Em490). Then, enzyme sample (400 ng recombinant ACAD9, VLCAD or ACAD9 chimera respectively) and human ETF (2 µM final concentration) in buffer 50 mM Tris-HCl, 0.5% w/v glucose, pH 8.0 were added. When applicable, 1mM FAD final concentration was added to the reaction mixture. Background fluorescence was recorded for 1 min. The reaction was initiated by addition of 30 µM final concentration of palmitoyl Acyl-CoA substrate (Sigma P9716) and immediately read for 120 s. Each experiment was performed in 3 to 6 replicates.

Statistical analysis

For BiFc and acyl-CoA activity assays, every sample of three to six independent experiments was presented as a mean average. Noted differences amongst the various sample types were assessed for significance. Statistically significant differences were determined by one-way ANOVA with Geisser-Greenhouse variability correction followed by Tukey-Kramer post-test to identify pair wise differences. Differences were considered significant at $P < 0.005$ (**), $P < 0.0002$ (***), $P < 0.0001$ (****).Statistical analyses were carried out using GraphPad Prism version 8 (GraphPad Software).

Supplementary Figures

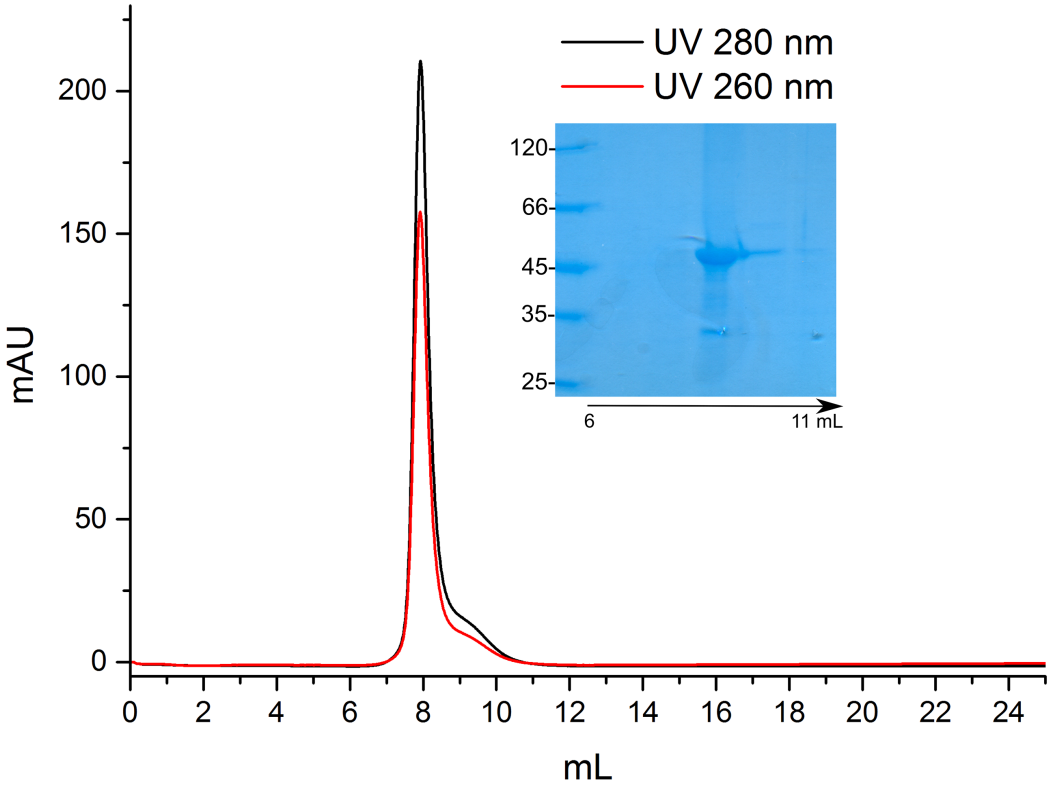

Figure S1. **Recombinant, purified mitochondrial ECSIT forms soluble aggregates.** SEC elution profile of the mitochondrial form of ECSIT (residues 49-431, 44kDa) monitored at two wavelengths, showing the elution of the protein main peak in the void volume of the SEC column (8mL). In the inset, SDS-PAGE gel showing the eluted fractions in the void volume (from 6 to 11 mL).

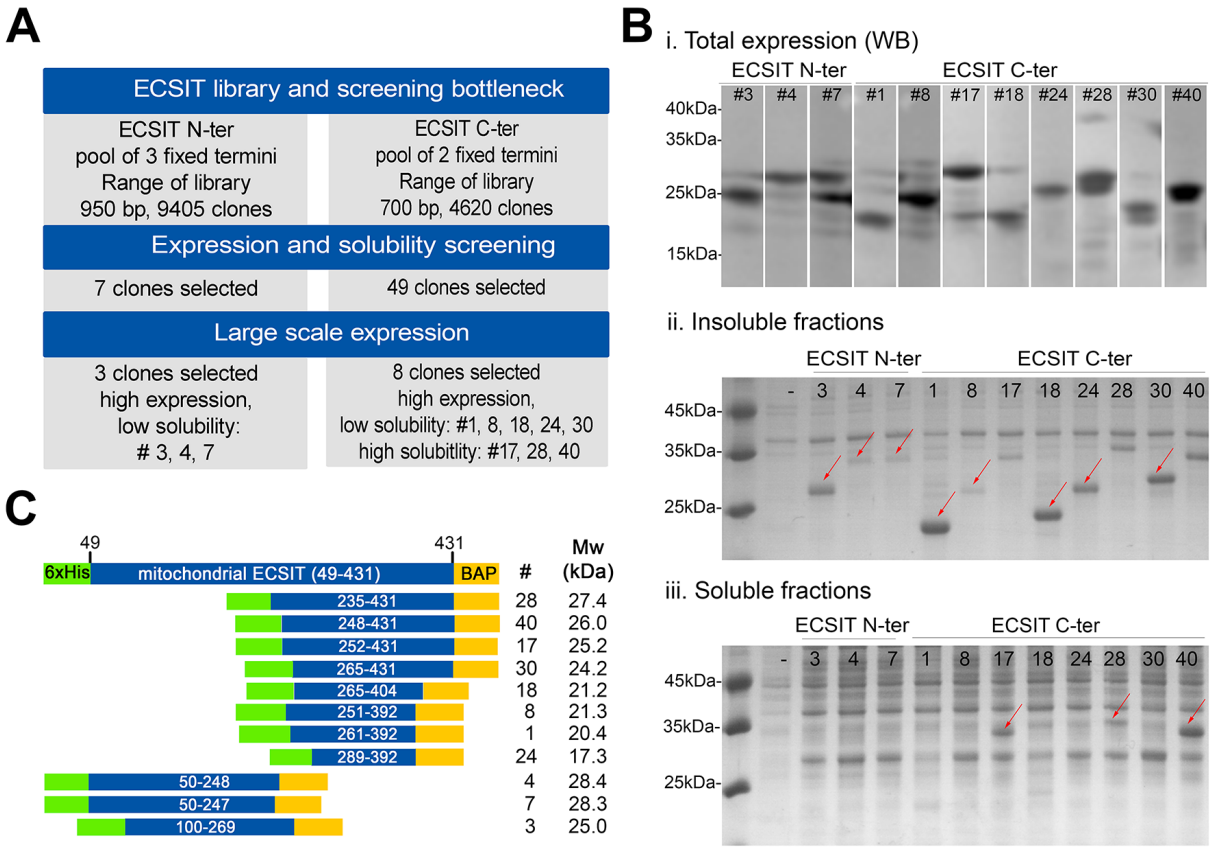

Figure S2. **Identification soluble fragments of ECSIT by the ESPRIT approach. A.** Schematic representation of the strategy for identifying soluble ECSIT domains: from a high-throughput screen of 9,405 and 4,620 clones corresponding to ECSIT N-terminal and C-terminal pools, respectively, 3 and 8 clones per each pool were selected for the scale-up. **B.** From the top, Western streptavidin blot against the C-terminal biotin acceptor peptide (BAP), insoluble and soluble fractions of protein fragments corresponding to N-terminal (clones #3, 4, 7) and C-terminal (clones #17, 18, 24, 28, 30 and 40) ECSIT. Red arrows indicate the proteins expressed as inclusion bodies or as soluble fractions, respectively. **C.** Summary of sequenced 3 N-terminal ECSIT and 8 C-terminal ECSIT clones. Construct boundaries are shown with the predicted molecular weights including 5 kDa from the hexahistidine (6xHis) and BAP tags.

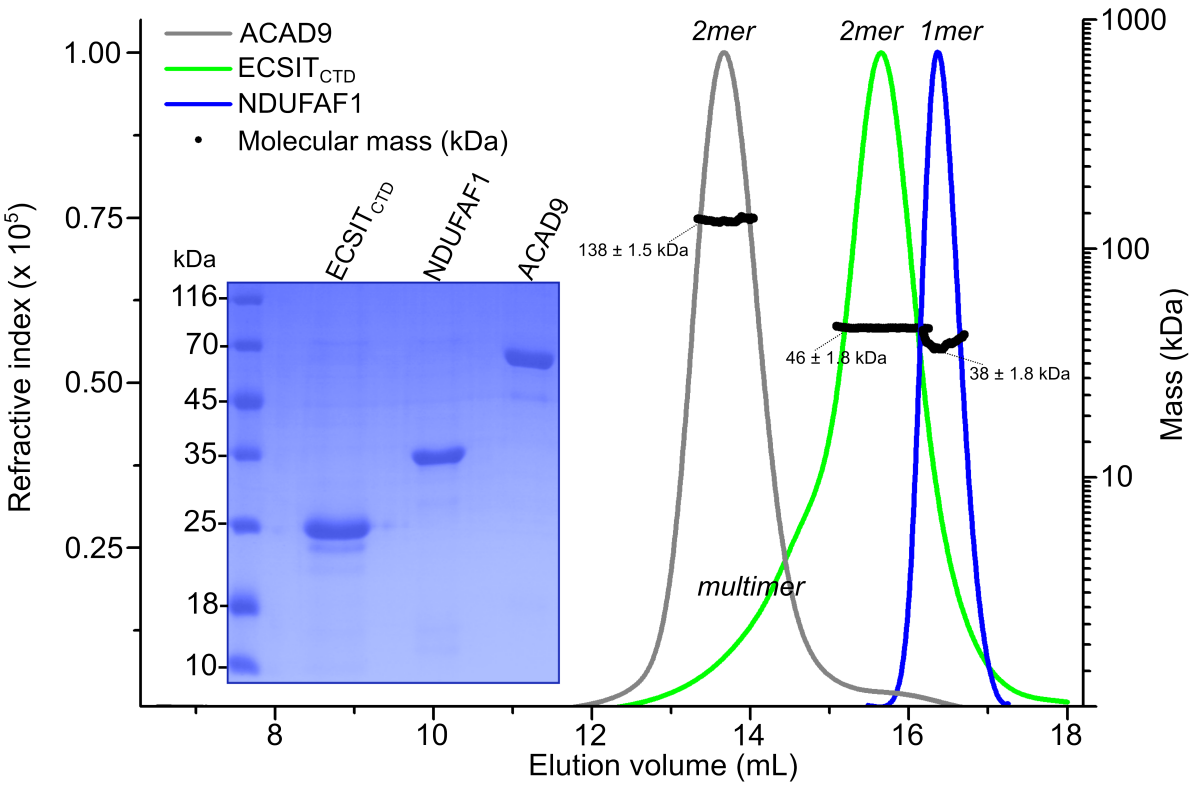

Figure S3. SEC-MALLS characterisation of recombinant ECSIT$_{CTD}$, NDUFAF1 and ACAD9. SEC elution profiles were monitored by excess refractive index (left ordinate axis). The black dots under each elution peak shows the molecular mass distribution (right ordinate axis). Measured molecular masses show that ACAD9 (grey line) is a 138 ± 1.5 kDa dimer, ECSIT$_{CTD}$ (green line) a 46 ± 1.8 kDa dimer and NDUFAF1 (blue line) a 38 ± 1.8 kDa monomer. In the inset, SDS-PAGE gel showing the purity and size of monomeric proteins in denaturing conditions.

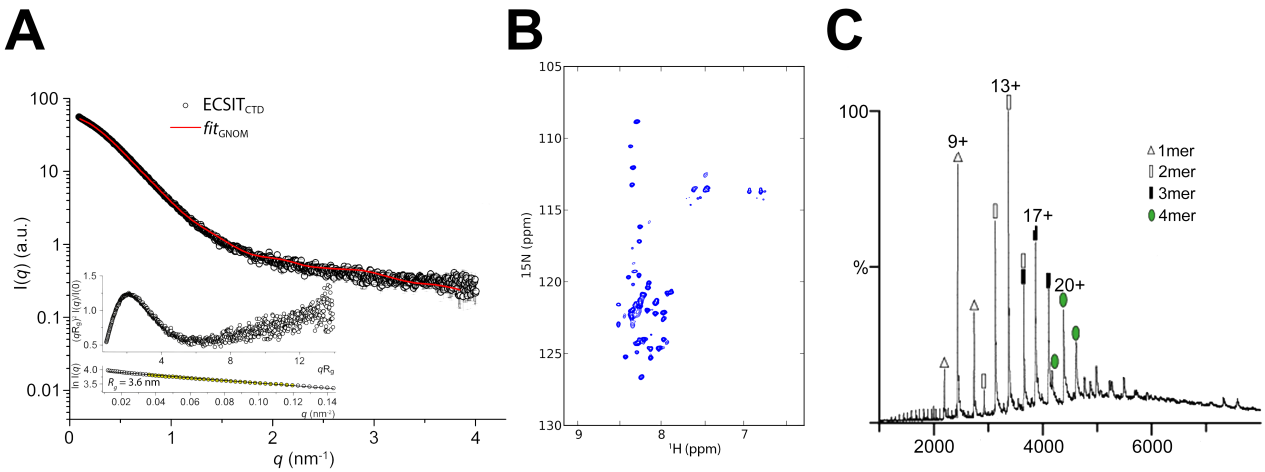

Figure S4. **ECSIT$_{CTD}$ is highly disordered and forms predominantly dimers**. **A.** SAXS experimental curve of ECSIT$_{CTD}$. In the inset, dimensionless Kratky plots and Guinier fit analyses, with an estimated mass of 46377 Da, corresponding to a dimer. **B.** ^{15}N-HSQC NMR spectrum of ^{15}N-labelled ECSIT$_{CTD}$ displays about 60 peaks in the amide region in a narrow ^{1}H frequency window corresponding to the amide random coil region showing that the residues observed by NMR belong to one or more unfolded parts of the protein. **C.** Native MS spectrum of ECSIT$_{CTD}$ with the detection of monomers (1mer, 21885 ±1 Da), dimers (2mer, 43771 ± 2 Da), tetramers (4mer, 87543 ±4 Da) and higher-order multimers.

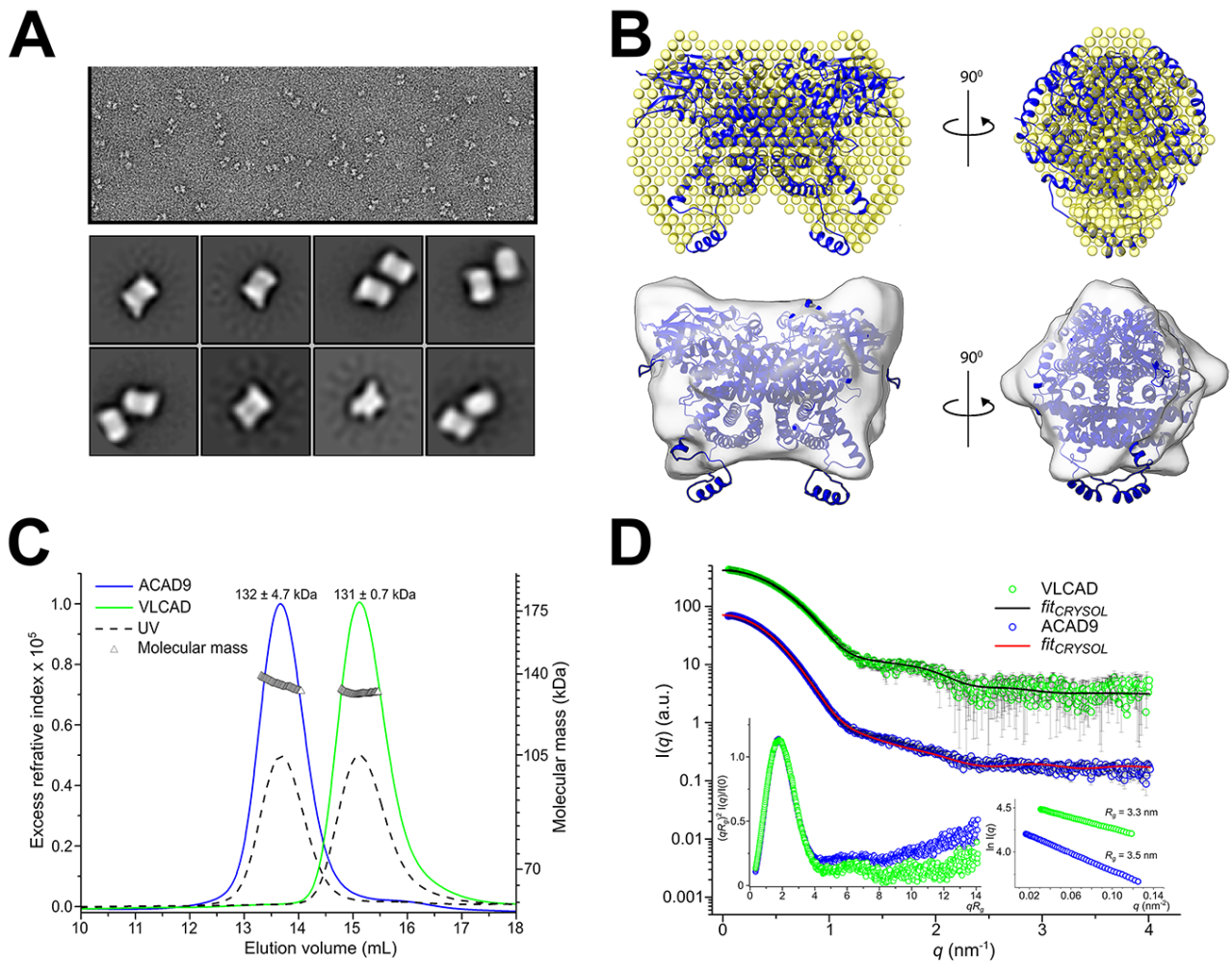

Figure S5. Conformational analysis of the ACAD9 homodimer. A. Ns-EM raw micrograph of ACAD9 particles and 2D class averages. **B.** *Top*, SAXS *ab initio* envelope for the ACAD9 dimer (bead model representation) matching the ACAD9 homology model (cartoon representation)[29]. *Bottom*, ns-EM map (grey) of ACAD9 fitted with the homology model. **C.** SEC-MALLS analysis of ACAD9 (residues 38-621, blue line) and VLCAD (residues 75-955, green line) by excess refractive index (left ordinate axis) and $UV_{280\ nm}$ wavelength (dotted lines). The triangular symbols under each elution peak show the molecular mass distribution (right ordinate axis), with ACAD9 as a 131 ± 0.7 kDa and VLCAD as a 132 ± 4.7 homodimers. **D.** X-ray scattering curves for ACAD9 and VLCAD (blue and green circles, respectively). *CRYSOL* fits using the ACAD9 homology model [29] and the VLCAD dimer crystal structure[30] represented as red lines (χ^2 values 2.5 and 0.92, respectively). In the inset, normalized Kratky plots (left) and close-up view of the Guinier region for the two proteins (right).

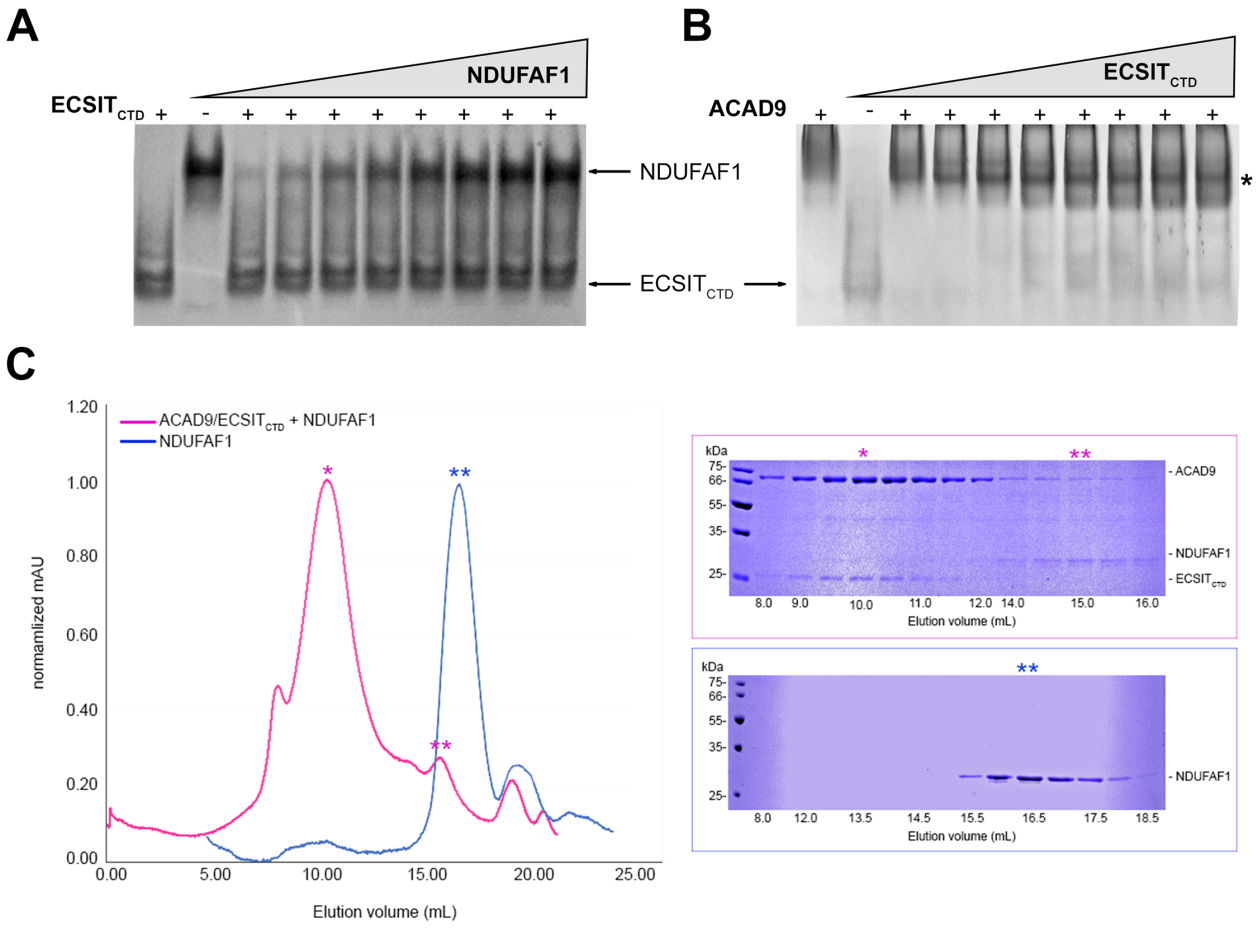

Figure S6. ***In vitro*** **interaction assays between ACAD9, ECSIT$_{CTD}$ and NDUFAF1. A.** ECSIT$_{CTD}$ when titrated with increasing NDUFAF1 concentrations shows no change in mobility. **B.** In contrast, ACAD9 titrated with increasing concentrations of ECSIT$_{CTD}$ shows the appearance of a new band, concomitant with the disappearance of the free ECSIT$_{CTD}$ band, revealing an interaction (*). **C.** On the left, UV$_{280nm}$ SEC elution profile of NDUFAF1 incubated with ACAD9-ECSIT$_{CTD}$ copurified complex (pink line). Comparison with the overlapped elution profile of NDUFAF1 alone (blue line) indicates that the main elution peak of the former profile corresponds to the ACAD9-ECSIT$_{CTD}$ complex (*), consistent with **Figure 2A**, with a small adjacent peak corresponding to unbound NDUFAF1 (**). The absence of a shift in the ACAD9-ECSIT$_{CTD}$ complex peak in presence of NDUFAF1 further confirms that NDUFAF1 is unable to form a complex with ACAD9-ECSIT$_{CTD}$. SDS-PAGE gels of the eluted fractions are shown on the right. *Top*, fractions from the gel filtration upon incubation of the three proteins. *Bottom*, fractions corresponding to the gel filtration of NDUFAF1 alone. Fractions corresponding to the peaks are highlighted with *.

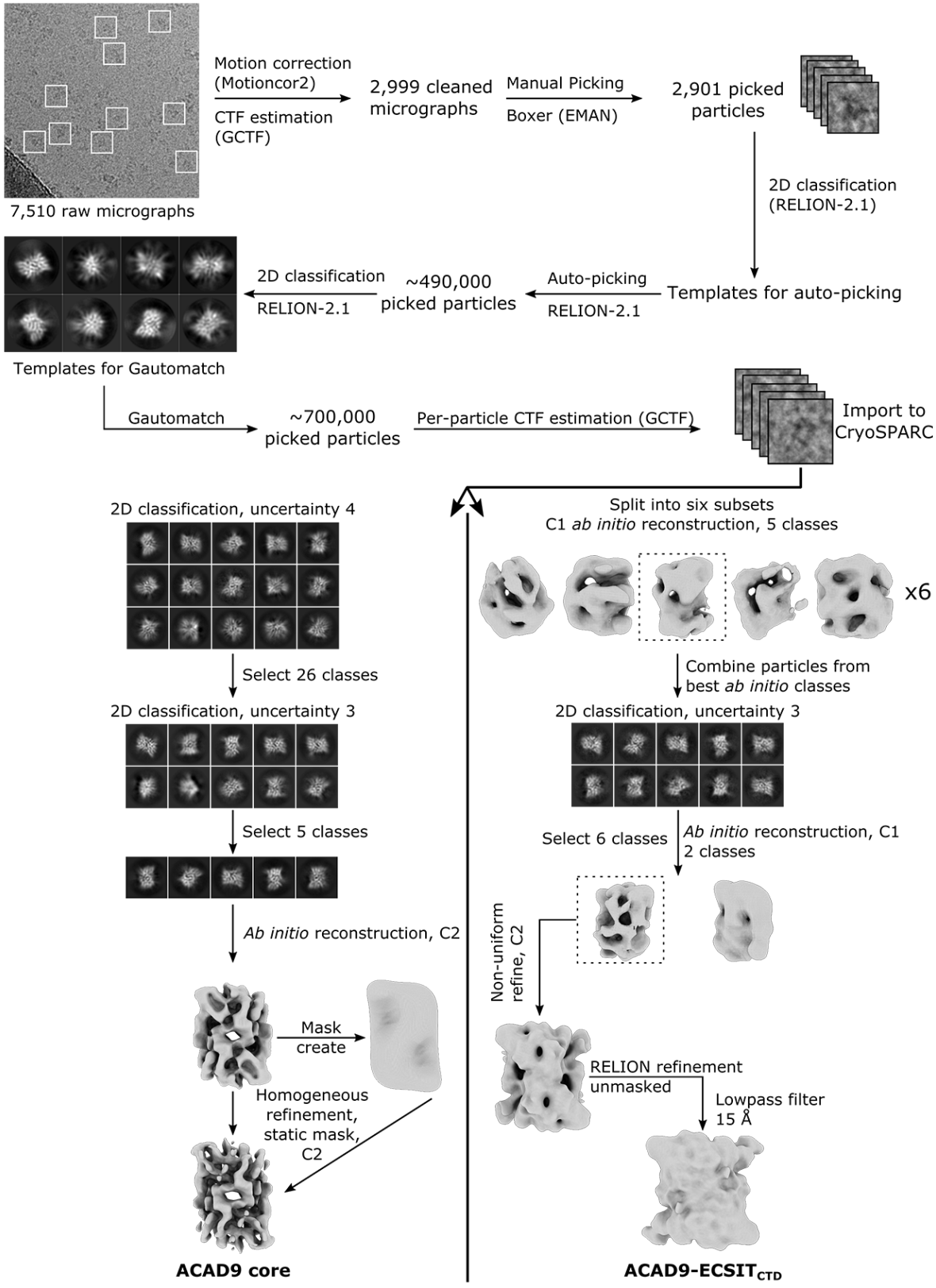

Figure S7. Cryo-EM processing strategy. Image processing pipeline of cryo-EM data for ACAD9-ECSIT$_{CTD}$ with software packages and algorithms used at each step indicated, for both the ACAD9 core and ACA9-ECSIT$_{CTD}$ maps.

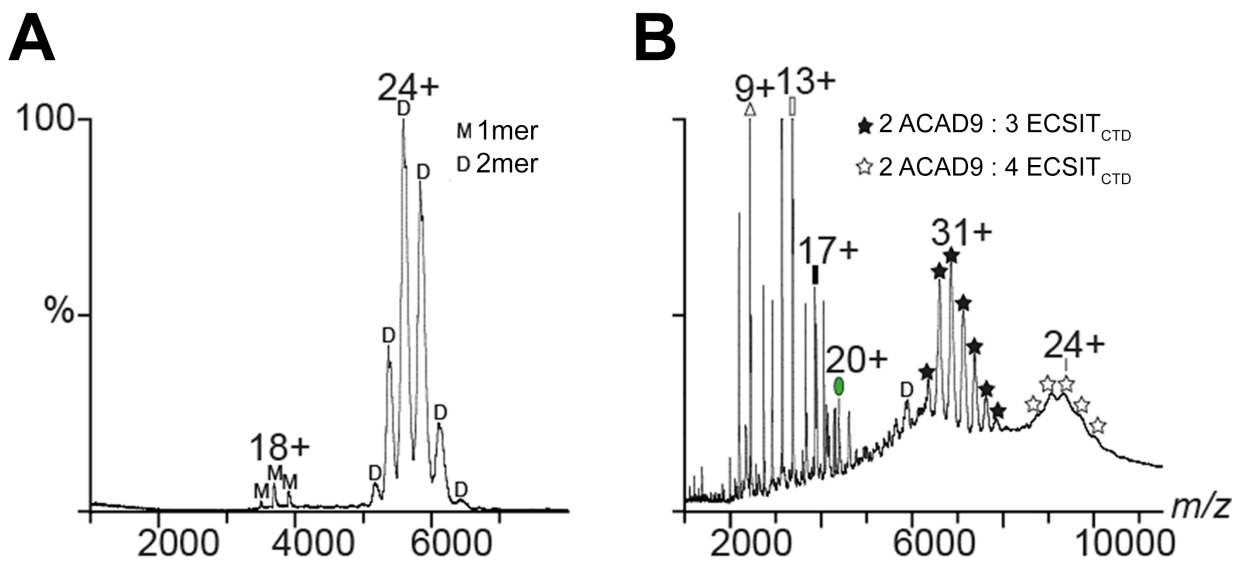

Figure S8. Investigation of different complex assemblies by Native MS. A. Mass spectrometric analysis of ACAD9 confirmed its homodimeric form (D 2mer, 131910 ± 4 Da); a very low abundant monomer was also detected (M 1mer, 65957 ± 3 Da). **B.** The copurified ACAD9-ECSIT$_{CTD}$ sample used in the cryo-EM experiments. Two major non-covalent species were characterised with a stoichiometry of an ACAD9 homodimer and 3 to 4 copies of ECSIT$_{CTD}$ (masses of 197,561 ± 3 Da and 219,457 ± 4 Da respectively). A series of additional peaks were detected consistent with the spectrum of unbound ECSIT$_{CTD}$ shown in **Figure S4C**, revealing the tendency of ECSIT$_{CTD}$ to form higher-order multimeric species in solution.

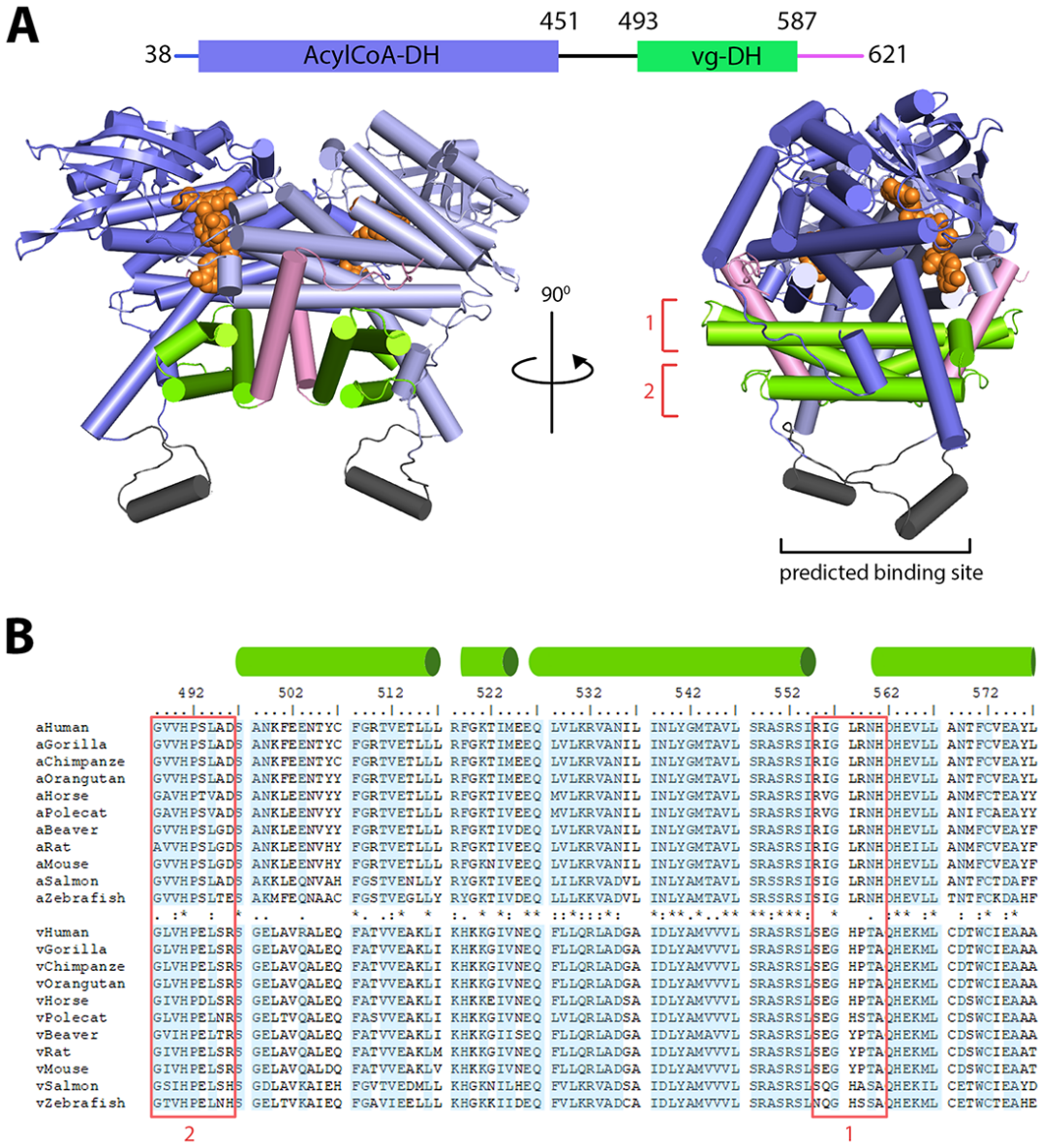

Figure S9. Structural features of the ACAD9 homodimer and potential interaction sites. A. *Top.* Domain organization of ACAD9, showing the Acyl-Coa (purple) and the vestigial (vg, green) dehydrogenase domains. *Bottom*. Two orientations of the ACAD9 homodimer *in silico* model[29] based on the VLCAD crystal structure[30]. The DH domain is shown in purple, the vg domain in green and the C-terminal segment responsible of homodimerization in pink. The C-terminal stretch of residues linking the DH and vg domains is shown in grey, poorly conserved between ECSIT and VLCAD and previously predicted to fold as a helix and be a potential protein-binding site[29]. Bound FAD is shown as orange spheres. **B.** Multiple sequence alignment of ACAD9 (a) and VLCAD (v) orthologues. Conserved residues between ACAD9 and VLCAD are highlighted in light blue. The regions corresponding to ACAD9 sequences $_{488}$GVVHPSLAD$_{496}$ and $_{555}$RIGLRNH$_{561}$ are boxed (1 and 2), highlighting the conservation of these sequences within ACAD9 and VLCAD orthologues and the divergence between the two groups.

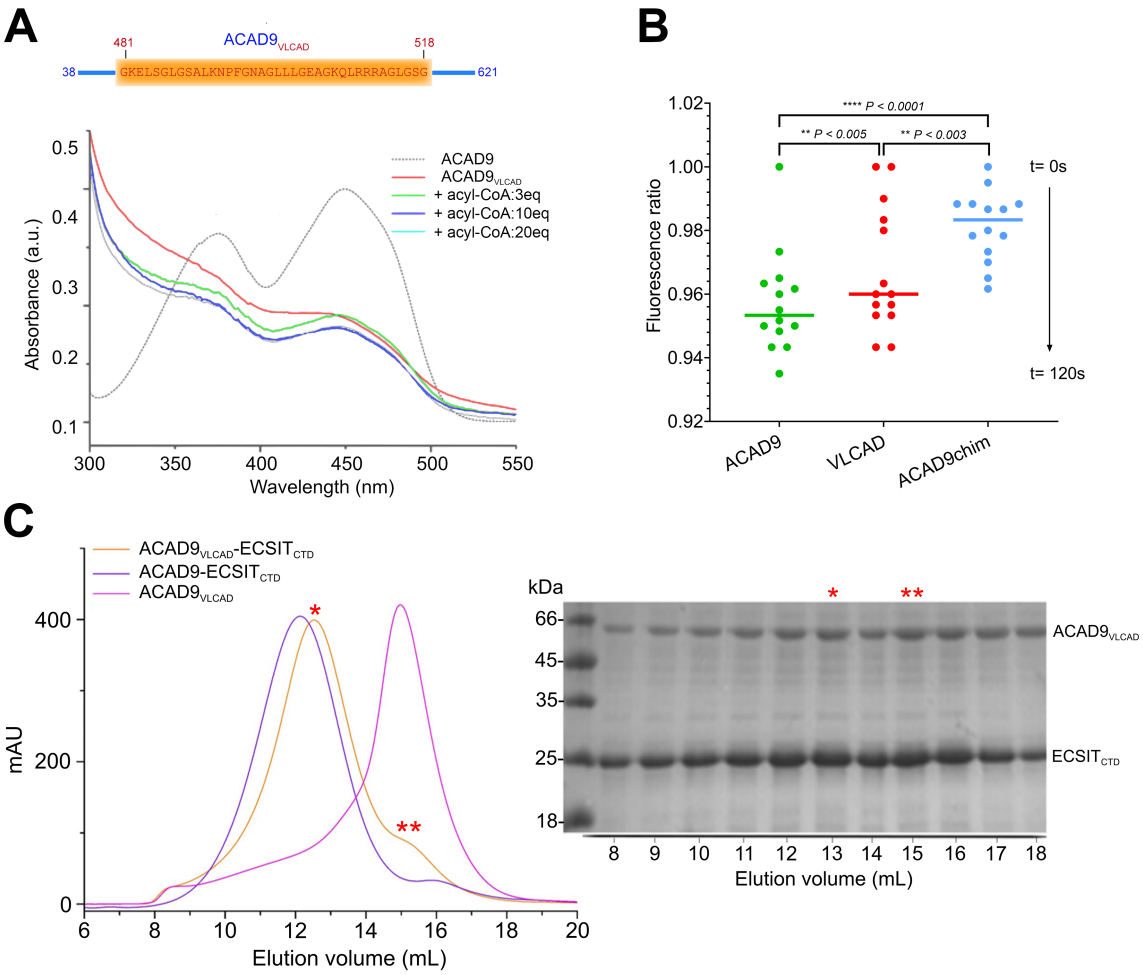

Figure S10. Construction of a VLCAD-based chimeric ACAD9 and its ability to bind to ECSIT$_{CTD}$. A. Design of a VLCAD-based ACAD9 chimeric mutant by swapping the C-terminal non-conserved 37 amino acid (residues 481 to 518) from VLCAD into ACAD9 (replacing residues 445 to 482). UV absorption spectra of ACAD9 (dashed line), showing absorption maxima near 370 and 450 nm, which are characteristic of oxidized FAD. The spectra of FAD bound to ACAD9$_{VLCAD}$ (red line) and 120 s after the addition of 1, 3, 10, 20 molar equivalent of acyl-CoA substrate (blue and green lines), showing no quenching of the absorption peaks in contrast to expected from the reduction of FAD into $FADH_2$. **B.** ACAD9$_{VLCAD}$ chimera shows a reduced loss of ETF fluorescence in presence of acyl-CoA substrate as compared to VLCAD and especially to ACAD9, indicating that ACAD9$_{VLCAD}$ has a perturbed dehydrogenase activity. **C.** SEC elution profile at 280 nm UV wavelength during the co-purification of the ACAD9$_{VLCAD}$-ECSIT$_{CTD}$ complex (orange line) showing a main elution peak corresponding to the complex (*) and a small adjacent peak to unbound ECSIT$_{CTD}$ (**). Overlapping of the elution profiles of the ACAD9-ECSIT$_{CTD}$ complex (purple line) and ACAD9$_{VLCAD}$ alone (magenta line) clearly indicate that there is a shift for the ACAD9$_{VLCAD}$-ECSIT$_{CTD}$ co-elution, providing evidence that ACAD9$_{VLCAD}$ is still able to form a complex with ECSIT$_{CTD}$. On the right, SDS-PAGE gel of the eluted fractions.

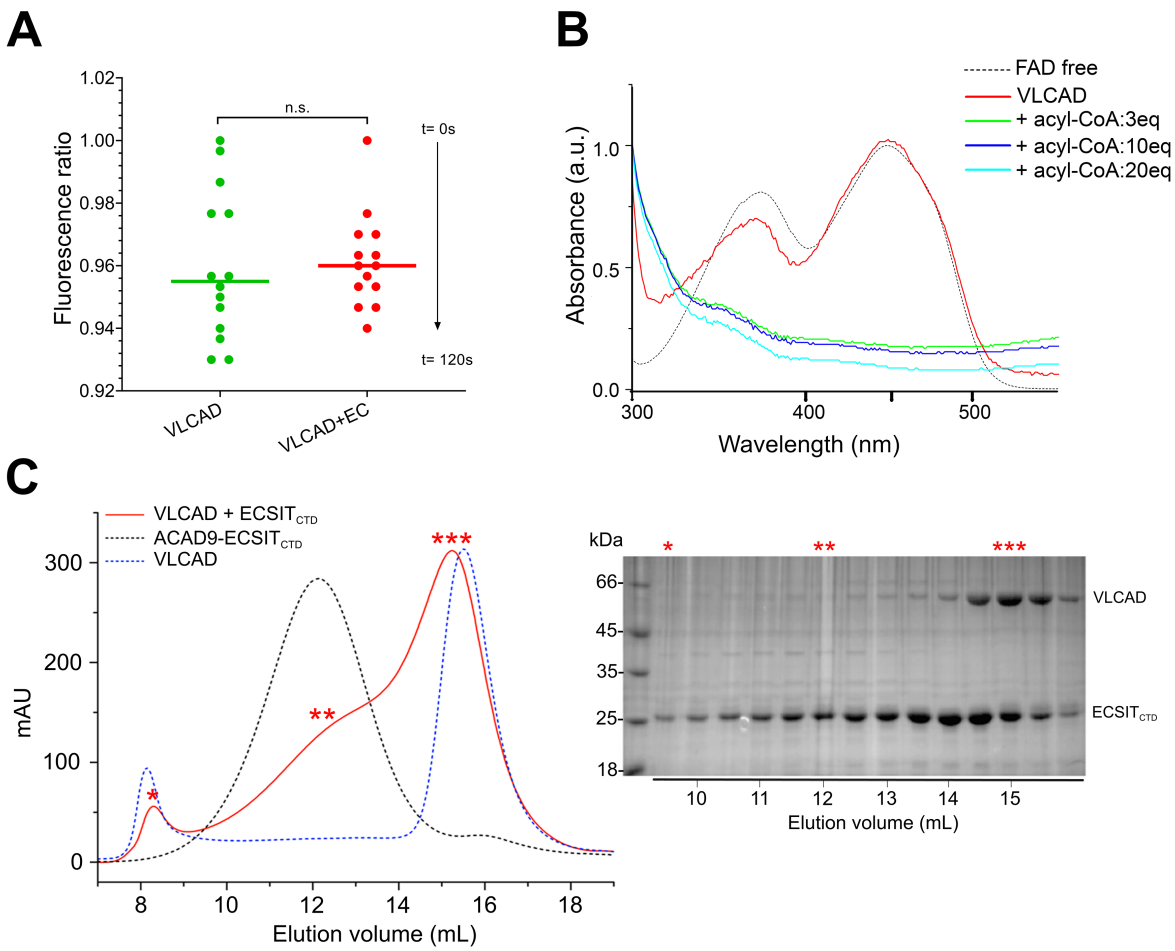

Figure S11. VLCAD enzymatic activity and its ability to bind to ECSIT$_{CTD}$. A. The dehydrogenase activity of VLCAD in presence acyl-CoA substrate is not affected by the presence of ECSIT$_{CTD}$, in contrast to ACAD9 (see **Figure 4**). **B.** UV absorption spectra of free FAD (dashed line), showing absorption maxima near 370 and 450 nm, which are characteristic of oxidized FAD. The spectra of FAD bound to VLCAD (red line) and 2 min after the addition of 1, 3, 10, 20 molar equivalent of acyl-CoA substrate (blue and green lines). Quenching of the absorption peaks results from the reduction of FAD into $FADH_2$ and provides evidence for the formation of a charge transfer complex with the electron acceptor ETF. **C.** SEC elution profile monitored at two UV wavelengths (280 and 260 nm) during the co-purification of VLCAD and ECSIT$_{CTD}$ showing three main elution peaks corresponding to the void volume (*), higher oligomeric species of ECSIT$_{CTD}$ (**) and VLCAD with an excess of ECSIT$_{CTD}$ (***). Overlapping of the elution profiles of the ACAD9-ECSIT$_{CTD}$ complex (black dash line) and VLCAD alone (blue dash line) indicate that there is no complex formation between VLCAD and ECSIT$_{CTD}$. On the right, SDS-PAGE gel of the eluted fractions.

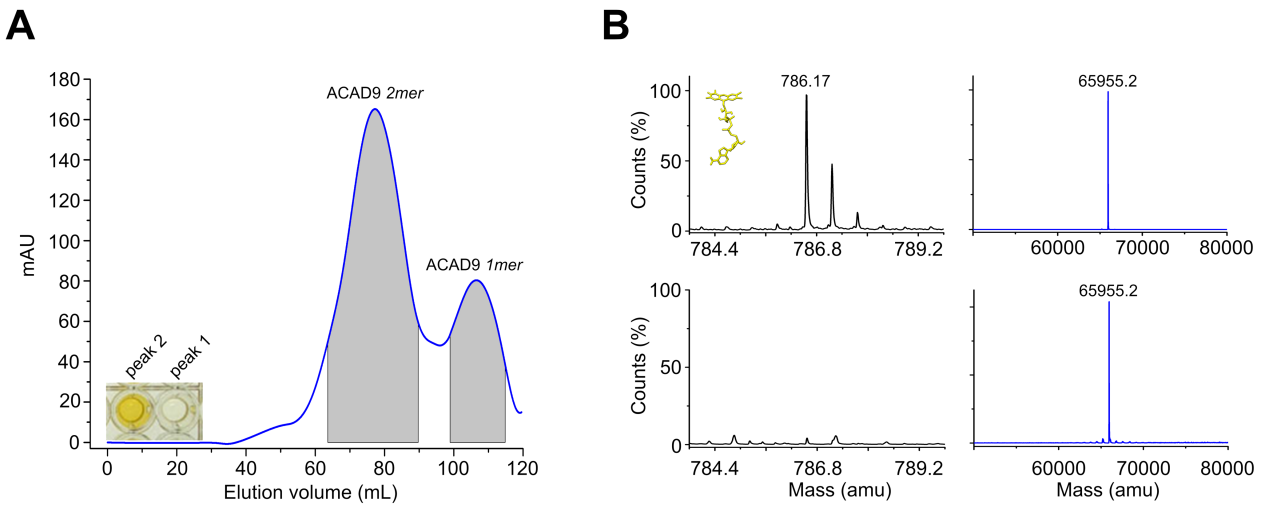

Figure S12. The ability of ACAD9 homodimer to bind FAD assessed by UV and MS. **A.** Only ACAD9 homodimer is able to bind FAD. SEC elution profile of full-length ACAD9 (residues 38-621) monitored at $UV_{280\ nm}$ during purification with preparative SEC showing two main elution peaks corresponding to ACAD9 dimer (peak 2, yellowish) and monomer (peak 1, colourless). **B.** LC/ESI-MS spectra of ACAD9 acquired after preparative SEC purification. In the upper panels, signals corresponding to the FAD cofactor (observed *m/z* 786.17 Da) and to ACAD9 (observed deconvoluted mass 65955.2 Da) eluted in chromatographic peak 2 (*2mer,* panel A) confirmed that ACAD9 homodimer binds FAD. In the lower panel, MS data indicated the absence of FAD when ACAD9 is a monomer.

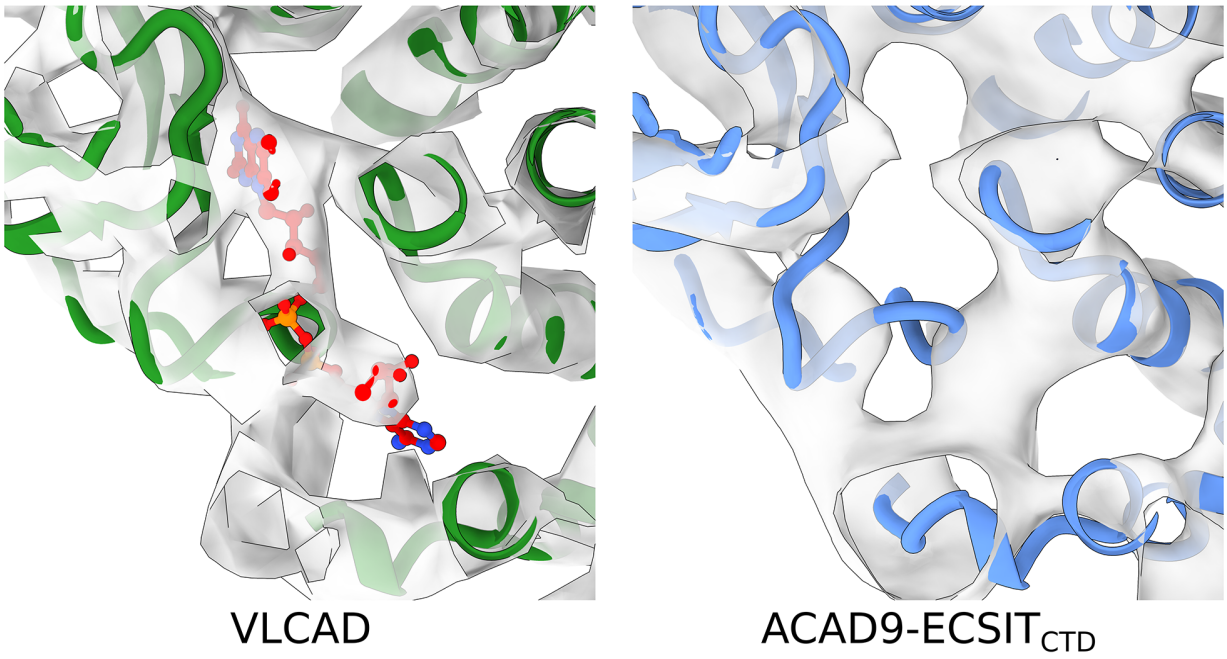

Figure S13. The FAD binding site in the ACAD9-ECSIT$_{CTD}$ complex is empty. Close-up views of the VLCAD crystal structure electron density map (PDB ID: 3B96[30]) filtered to 8 Å resolution showing the bound FAD in ball-and-sticks (left) and of the ACAD9 core of the ACAD9-ECSIT$_{CTD}$ cryo-EM map at the same resolution (right), showing the absence of an FAD density in the catalytic binding site of the ACAD9-ECSIT$_{CTD}$ complex.

Supplementary Table

Table S1. SAXS data of the proteins and protein fragments of this study.

(a) **Sample details.**

	$ECSIT_{CTD}$	**NDUFAF1**	**ACAD9**	**Chimeric $ACAD9_{VLCAD}$**	**VLCAD**	**ACAD9-$ECSIT_{CTD}$ complex**
UniProt sequence ID (residues in construct)	Q9BQ95 (247-431)	Q9Y375 (25-327)	Q9H845 (38-621)	Δ_{ACAD9} 445-482/$_{VLCAD}$ 481-518	P49748 (75-655)	Q9BQ95 (247-431) and Q9H845 (38-621)
Particle contrast from sequence and solvent constituents, $\Delta\rho(\rho_{protein} - \rho_{solvent}; 10^{10}; cm^{-2})$	2.949 (12.44-9.49)	2.878 (12.37-9.49)	2.744 (12.24-9.49)	2.744 (12.24-9.49)	2.732 (12.23-9.49)	n.d.
Specific volume from chemical composition (v, $cm^3\ g^{-1}$)	0.726	0.732	0.742	0.742	0.742	n.d.
Calculated monomeric mass from sequence (Da)	21887.20	35131.50	65954.82	65456.17	64040.65	n.d.
Total frames	10		2400			10
Frames used for data analysis	10		60 (range 2280-2340)	100 (range 1900-2000)	100 (range 2080-2180)	10

(b) **SAXS data collection parameters**

Instrument	ESRF, Grenoble (France), bioSAXS beamline (BM29)		
Wavelength (Å)	0.99		
q-range ($Å^{-1}$)	0.004 – 0.49		
Sample-to-detector distance (m)	2.864		
Exposure time (sec)	0.5/frame	1/frame	0.5/frame
Temperature (° C)	20		
Detector	Pilatus 1M		
Flux (photons/s)	2 x 10^{12}		
Beam size (μm^2)	700 x 700		
Sample configuration	1.8 mm quartz glass capillary		
Absolute scaling method	Comparison to water in sample capillary		
Normalization	To transmitted intensity by beam-stop counter		
Monitoring for radiation damage	Control of un-subtracted and scaled subtracted data for systematic changes typical for radiation damage		

(c) **Structural parameters**

	$ECSIT_{CTD}$	**NDUFAF1**	**ACAD9**	**Chimeric $ACAD9_{VLCAD}$**	**VLCAD**	**ACAD9-$ECSIT_{CTD}$ complex**
Guinier analysis						
I(0) (cm^{-1})	0.042 ± 9.6E-05	0.029 ± 1.8E-04	0.057 ± 2.5E-05	0.11 ± 1.1E-04	0.107 ± 8.E-06	0.190 ± 2.8E-05
R_g (nm)	3.53 ± 0.041	2.85 ± 0.023	3.54 ± 0.011	3.85 ± 0.042	3.36 ± 0.024	6.09 ± 0.031
q range (nm^{-1})	0.0362-0.1170	0.0173-0.1550	0.0160-0.1087	0.0325-0.1008	0.0352-0.1494	0.0056-0.0423

Auto R_g fidelity	0.98	0.96	0.99	0.95	0.99	0.96
Mass from I(0) (Da); ratio to predicted	46473.3; 2.1	37700; 1.07	113650; 1.7	131078; 1.98	130875;2.04	289822; n.d.
P(r) analysis						
I(0) (cm^{-1})	0.04236	0.02924	0.056736	0.11096	0.10704	0.19024
R_g (nm)	3.65	2.9	3.51	3.7	3.31	5.97
D_{max} (nm)	11.9	10	11.34	11.7	9.8	18.3
q range (nm^{-1})	0.207-3.53	0.282-2.912	0.118-3.827	0.192-3.12	0.213-3.5	0.101-2.952
Porod volume (nm^3)	116.82	79.29	234	220	233	678
Porod exponent (from Scåtter)	1.3	1.1	2.3	2.7	2.9	2.4
Mass estimate (as 0.5 x volume of models, Da); ratio to expected	58410; 2.61	39645; 1.12	117000; 1.8	110000; 1.7	116500; 1.8	339000
Mass from I(0) (Dalton); ratio to predicted	46377; 2.12	31740; 0.9	126800; 1.92	125930; 1.9	125492; 1.95	289737; n.d.
SASBDB Accession ID	SASDHU4	SASDHV4	SASDHW4	SASDHX4	SASDHY4	SASDHZ4

***(d)* Shape model-fitting results.**

DAMMIF	*Default parameters, 20 calculation runs*					
q range (nm^{-1})	0.067-2.8	0.17-2.94	0.099-4.270	0.064-3	0.184-4.262	0.068-2.149
Symmetry, anisotropy assumptions	P2, none	P1, none	P2, none	P2, none	P2, none	P2, none
Normalized spatial discrepancy (standard deviation)	1.304 (0.174)	0.696 (0.026)	1.377 (0.205)	1.607 (0.228)	1.001 (0.268)	1.803 (0.268)
Resolution (from SASRES) (Å)	39 ± 3	23 ± 2	57 ± 4	57 ± 4	41 ± 3	88 ± 6
χ^2 range of the fitting	1.142-1.169	2.482-2.498	1.852-1.921	3.347-3.542	0.408-0.427	1.137-1.207
DAMMIN	*Default parameters, fine, smaller beads*					
q range (nm^{-1})	0.067-2.8	0.17-2.94	0.099-4.270	0.064-3	0.184-4.262	0.068-2.149
Symmetry, anisotropy assumptions	P2, none	P1, none	P2, none	P2, none	P2, none	P2, none
χ^2 value of the fitting	1.081	4.317	1.743	3.535	0.4217	1.238
GASBOR	*Default parameters, reciprocal space (fit I(s), slower)*					
q range (nm^{-1})	n.d.	n.d.	0.099-4.270	0.064-3	0.184-4.262	0.068-2.149
Symmetry, anisotropy assumptions	n.d.	n.d.	P2, none	P2, none	P2, none	P2, none
χ^2 value of the fitting	n.d.	n.d.	3.95	4.27	0.459	1.205

***(e)* Atomistic modelling.**

Atomic structures	n.d.	n.d.	Homology model (residues 38-621)$^+$	Homology model (residues 38-621)$^+$	PDB entry 3B96	n.d.
CRYSOL	*Default parameters, with constant subtraction*					
- χ^2 value of the fitting	n.d.	n.d.	2.55	8.70	0.92	n.d.
- Predicted R_g (nm)	n.d.	n.d.	3.50	3.50	3.30	n.d.

n.d.: non determined.

Supplementary References

[1] F. van den Ent, J. Lowe, *J Biochem Biophys Methods* **2006**, *67*, 67-74.
[2] P. J. Mas, D. J. Hart, *Methods Mol Biol* **2017**, *1586*, 45-63.
[3] A. Favier, B. Brutscher, *J Biomol NMR* **2011**, *49*, 9-15.
[4] F. Delaglio, S. Grzesiek, G. W. Vuister, G. Zhu, J. Pfeifer, A. Bax, *Journal of Biomolecular NMR* **1995**, *6*, 277-293.
[5] P. Pernot, A. Round, R. Barrett, A. De Maria Antolinos, A. Gobbo, E. Gordon, J. Huet, J. Kieffer, M. Lentini, M. Mattenet, C. Morawe, C. Mueller-Dieckmann, S. Ohlsson, W. Schmid, J. Surr, P. Theveneau, L. Zerrad, S. McSweeney, *J Synchrotron Radiat* **2013**, *20*, 660-664.
[6] M. E. Brennich, A. R. Round, S. Hutin, *J Vis Exp* **2017**.
[7] D. Franke, M. V. Petoukhov, P. V. Konarev, A. Panjkovich, A. Tuukkanen, H. D. T. Mertens, A. G. Kikhney, N. R. Hajizadeh, J. M. Franklin, C. M. Jeffries, D. I. Svergun, *Journal of Applied Crystallography* **2017**, *50*, 1212-1225.
[8] R. P. Rambo, J. A. Tainer, *Nature* **2013**, *496*, 477-481.
[9] D. I. Svergun, M. H. Koch, *Curr Opin Struct Biol* **2002**, *12*, 654-660.
[10] J. Trewhella, A. P. Duff, D. Durand, F. Gabel, J. M. Guss, W. A. Hendrickson, G. L. Hura, D. A. Jacques, N. M. Kirby, A. H. Kwan, J. Perez, L. Pollack, T. M. Ryan, A. Sali, D. Schneidman-Duhovny, T. Schwede, D. I. Svergun, M. Sugiyama, J. A. Tainer, P. Vachette, J. Westbrook, A. E. Whitten, *Acta Crystallogr D Struct Biol* **2017**, *73*, 710-728.
[11] P. V. Konarev, M. V. Petoukhov, D. I. Svergun, *J Appl Crystallogr* **2016**, *49*, 953-960.
[12] E. F. Pettersen, T. D. Goddard, C. C. Huang, G. S. Couch, D. M. Greenblatt, E. C. Meng, T. E. Ferrin, *J Comput Chem* **2004**, *25*, 1605-1612.
[13] E. Boeri Erba, C. Petosa, *Protein Sci* **2015**, *24*, 1176-1192.
[14] E. Boeri Erba, L. Signor, M. F. Oliva, F. Hans, C. Petosa, *Methods Mol Biol* **2018**, *1764*, 133-151.
[15] F. Sobott, H. Hernandez, M. G. McCammon, M. A. Tito, C. V. Robinson, *Anal Chem* **2002**, *74*, 1402-1407.
[16] N. Morgner, C. V. Robinson, *Anal Chem* **2012**, *84*, 2939-2948.
[17] A. Rohou, N. Grigorieff, *J Struct Biol* **2015**, *192*, 216-221.
[18] J. Zivanov, T. Nakane, B. O. Forsberg, D. Kimanius, W. J. Hagen, E. Lindahl, S. H. Scheres, *Elife* **2018**, *7*.
[19] E. Kandiah, T. Giraud, A. de Maria Antolinos, F. Dobias, G. Effantin, D. Flot, M. Hons, G. Schoehn, J. Susini, O. Svensson, G. A. Leonard, C. Mueller-Dieckmann, *Acta Crystallogr D Struct Biol* **2019**, *75*, 528-535.
[20] H. Peng, Z. Zhou, E. Meijering, T. Zhao, G. A. Ascoli, M. Hawrylycz, *Nat Methods* **2017**, *14*, 332-333.
[21] K. Zhang, *J Struct Biol* **2016**, *193*, 1-12.
[22] S. J. Ludtke, P. R. Baldwin, W. Chiu, *J Struct Biol* **1999**, *128*, 82-97.
[23] D. Kimanius, B. O. Forsberg, S. H. Scheres, E. Lindahl, *Elife* **2016**, *5*.
[24] A. Punjani, J. L. Rubinstein, D. J. Fleet, M. A. Brubaker, *Nat Methods* **2017**, *14*, 290-296.
[25] M. Soler-Lopez, A. Zanzoni, R. Lluis, U. Stelzl, P. Aloy, *Genome Res* **2011**, *21*, 364-376.
[26] Y. Min, S. M. Wi, D. Shin, E. Chun, K. Y. Lee, *Front Cell Infect Microbiol* **2017**, *7*, 94.
[27] Y. Zhang, A. W. Mohsen, C. Kochersperger, K. Solo, A. V. Schmidt, J. Vockley, E. S. Goetzman, *Anal Biochem* **2019**, *581*, 113332.
[28] J. Malecki, A. Y. Ho, A. Moen, H. A. Dahl, P. O. Falnes, *J Biol Chem* **2015**, *290*, 423-434.
[29] J. Nouws, L. Nijtmans, S. M. Houten, M. van den Brand, M. Huynen, H. Venselaar, S. Hoefs, J. Gloerich, J. Kronick, T. Hutchin, P. Willems, R. Rodenburg, R. Wanders, L. van den Heuvel, J. Smeitink, R. O. Vogel, *Cell Metab* **2010**, *12*, 283-294.
[30] R. P. McAndrew, Y. Wang, A. W. Mohsen, M. He, J. Vockley, J. J. Kim, *J Biol Chem* **2008**, *283*, 9435-9443.